

# Conductance quantization and snake states in graphene magnetic waveguides

T. K. Ghosh, A. De Martino, W. Häusler, L. Dell'Anna, and R. Egger  
*Institut für Theoretische Physik, Heinrich-Heine-Universität, D-40225 Düsseldorf, Germany*  
 (Dated: October 31, 2018)

We consider electron waveguides (quantum wires) in graphene created by suitable inhomogeneous magnetic fields. The properties of uni-directional snake states are discussed. For a certain magnetic field profile, two spatially separated counter-propagating snake states are formed, leading to conductance quantization insensitive to backscattering by impurities or irregularities of the magnetic field.

PACS numbers: 73.21.-b, 73.63.-b, 75.70.Ak

The physics of monolayer graphene devices has recently attracted a great deal of attention [1, 2]. From a fundamental perspective, one can hope to relate experimental observations to the mathematical properties of two-dimensional massless Dirac-Weyl quasiparticles. The pseudo-relativistic dispersion relation with Fermi velocity  $v_F \approx 10^6$  m/sec is intimately connected to the sublattice structure: the basis of the graphene honeycomb lattice contains two carbon atoms, giving rise to an isospin degree of freedom. Graphene has also been suggested as new material system for device applications [2]. In this paper, we pose (and affirmatively answer) the question whether quantum wires with quantized conductance can be formed in graphene. Such electron waveguides are indispensable parts of any conceivable all-graphene device. In lithographically formed graphene ‘ribbons’, the electronic bandstructure is theoretically expected to very sensitively depend on the width and on details of the boundary [3]. On top of that, disorder and structural inhomogeneity are substantial in real graphene [4]. For narrow graphene ribbons or electrostatically formed graphene wires [5], conventional conductance quantization thus seems unlikely [6]. This expectation is in accordance with recent experiments [7].

Contrary to such pessimism, we here demonstrate that by designing a suitable *inhomogeneous* magnetic field, a magnetic waveguide can be built that indeed allows for the perfectly quantized two-terminal conductance  $4e^2/h$  (including spin and valley degeneracy) even when disorder is present. The disorder insensitivity is based on a spatial separation of the left- and right-moving ‘snake’ states found under the model geometry shown in Fig. 1(a). This is reminiscent of the edge states encountered in the integer quantum Hall regime [8], but here refers to a completely different microscopic picture. Such *double-snake states* develop in the regime  $B > 0$  but  $B' < 0$ , while an individual snake state is uni-directional and already found in the setup of Fig. 1(b). Magnetic barrier technology is well developed [9, 10, 11] and its application to graphene samples appears to pose no fundamental problems [12]. In fact, snake states were experimentally studied in other materials [9, 13], mainly motivated by the quest for electrical rectification. On the theory side, for Schrödinger fermions, the magnetic field profile in Fig. 1(a) (but only for  $B' = 0$ ) was discussed

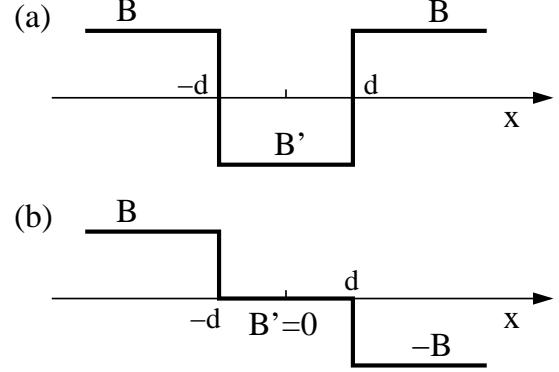


FIG. 1: Magnetic field profile (2) for magnetic waveguide (homogeneous along  $y$  direction). (a) Case  $\sigma = 1$ . For  $B' < 0$ , counter-propagating pairs of snake states are possible. (b) Case  $\sigma = -1$ , with uni-directional propagating snake states.

in Ref. [14], and asymmetric cases as in Fig. 1(b) were studied by a number of authors [15]. For the Dirac-Weyl quasiparticles encountered in graphene, however, such calculations were not reported. Inhomogeneous magnetic fields in graphene were discussed by several of us [16], and we employ that framework in our proposal of magnetic waveguides in graphene.

For a static orbital magnetic field with perpendicular component  $B(x, y)$ , the time-independent Dirac-Weyl equation for the quasiparticle isospinor  $\Psi(x, y)$  at energy  $E = v_F \epsilon$  reads (we put  $\hbar = 1$ )

$$\boldsymbol{\sigma} \cdot \left( -i \boldsymbol{\nabla} + \frac{e}{c} \mathbf{A} \right) \Psi = \epsilon \Psi, \quad (1)$$

where following Ref. [16], we focus on a single  $K$  point (valley). The Pauli matrices  $\sigma_\alpha$  with  $\boldsymbol{\sigma} = (\sigma_1, \sigma_2)$  act in sublattice space, and  $B(x, y) \hat{e}_z = \text{rot} \mathbf{A}(x, y)$ . The field profiles considered in Fig. 1 are independent of the longitudinal transport direction  $y$  and constant within each of the three regions,

$$B(x) = \begin{cases} B, & x < -d, \\ B', & |x| < d, \\ \sigma B, & x > d, \end{cases} \quad (2)$$

where  $\sigma = \pm 1$  gives the relative sign of the magnetic field on the two sides  $|x| > d$ . We mention in passing that we

have also studied the power-law form  $B(x) \propto x^m$  (with  $m = 1, 2, 3$ ) to make sure that the steps in Eq. (2) do not cause unphysical artefacts. Indeed the same qualitative features as reported below for the profile (2) were found from such calculations, which can also benefit from the semi-classical approximation. A convenient gauge for the vector potential,  $\mathbf{A} = A(x)\hat{e}_y$  with  $B(x) = \partial_x A(x)$ , is (for  $\sigma = +1$ )

$$A(x) = \begin{cases} Bx + (B - B')d, & x < -d, \\ B'x, & |x| < d, \\ Bx - (B - B')d, & x > d. \end{cases} \quad (3)$$

Due to translation invariance in the  $y$ -direction, we can parametrize solutions  $\Psi(x, y) = \psi(x)e^{iky}$  by the conserved longitudinal momentum  $k$ . From Eq. (1), for the spinor component  $u$  in  $\psi(x) = (u, v)^T$ , we obtain

$$\left[ \partial_x^2 - \frac{e}{c}B(x) - \left( k + \frac{e}{c}A(x) \right)^2 + \epsilon^2 \right] u = 0. \quad (4)$$

For  $\epsilon \neq 0$ ,  $v = \frac{1}{i\epsilon}[\partial_x - k - \frac{e}{c}A(x)]u$  then gives the other component. To obtain the bandstructure, we first determine the general solution in each of the three regions separately. Matching conditions follow from the continuity of the wavefunction at  $x = \mp d$  and will be shown to give an energy quantization condition.

For  $x < -d$ , the constant magnetic field  $B$  implies the lengthscale  $l_B = \sqrt{c/e|B|}$ . We may then explicitly solve Eq. (4) in terms of parabolic cylinder functions  $D_p(q)$  [16]. With the auxiliary variables

$$q = \sqrt{2}[(x+d)/l_B + \text{sgn}(B)kl_B], \quad p = (\epsilon l_B)^2/2 - 1, \quad (5)$$

and complex coefficients  $a_{\pm}$ , the solution reads

$$\psi_{B>0}(x) = \sum_{\pm} a_{\pm} \begin{pmatrix} D_p(\pm q) \\ \mp \frac{\sqrt{2}}{i\epsilon l_B} D_{p+1}(\pm q) \end{pmatrix}, \quad (6)$$

$$\psi_{B<0}(x) = \sum_{\pm} a_{\pm} \begin{pmatrix} D_{p+1}(\pm q) \\ \pm \frac{\sqrt{2}}{i\epsilon l_B} (p+1) D_p(\pm q) \end{pmatrix}. \quad (7)$$

Similarly, the eigenfunction for  $x > d$  can be expressed with coefficients  $c_{\pm}$ , and replacing  $d \rightarrow -d$  in Eq. (5). Finally, for  $B' \neq 0$ , the region  $|x| < d$  again admits such a representation with coefficients  $b_{\pm}$  and  $d \rightarrow 0$  in Eq. (5). For  $B' = 0$ , a plane-wave solution applies instead,

$$\psi(x) = \sum_{\pm} b_{\pm} \begin{pmatrix} 1 \\ \frac{\pm k_{\perp} + ik}{\epsilon} \end{pmatrix} e^{\pm ik_{\perp}(x+d)}, \quad (8)$$

where  $k_{\perp} = \sqrt{\epsilon^2 - k^2}$ . For  $|\epsilon| < |k|$ , the square root is taken as  $k_{\perp} = i\sqrt{|\epsilon^2 - k^2|}$ . Without loss of generality we now put  $B > 0$ . Normalizability then implies  $a_+ = c_{-\sigma} = 0$  and we are left with four complex coefficients, one of which is fixed by the normalization condition. The two matching conditions (at  $x = \mp d$ ) for the 2-spinor  $\psi(x)$  then give 4 equations for 3 unknowns, which generates the sought condition for the energy bands  $\epsilon_n(k)$ .

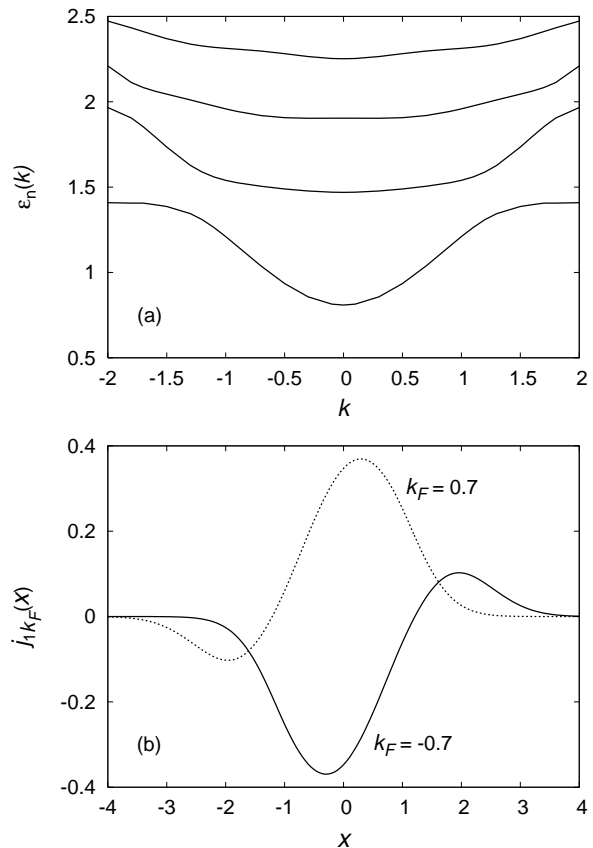


FIG. 2: (a) Spectrum of the magnetic waveguide with  $\sigma = +1$ ,  $d = l_B$  and  $B' = 0$ . Energies (momenta) are given in units of  $v_F/l_B$  ( $l_B^{-1}$ ). Only the few lowest electron-like ( $\epsilon_n(k) > 0$ ) states are shown. (b) Current profile  $j_{1k_F}(x)$  in units of  $v_F/l_B$ , see Eq. (11), with  $x$  in units of  $l_B$ . The plot is for  $n = 1$  and  $\epsilon l_B = 1$ , leading to  $k_F l_B \simeq \pm 0.7$ . The two counter-propagating states are centered near the middle of the waveguide.

For the *symmetric* setup  $\sigma = +1$  with  $B' = 0$ , some algebra yields the energy quantization condition

$$w^{-1}(u_2 v_1 - z^2 u_1 v_2) + w(z^2 u_2 v_1 - u_1 v_2) + (z^2 - 1)(u_1 u_2 - v_1 v_2) = 0, \quad (9)$$

which for given  $k$  generates an equation for  $\epsilon$  since  $k_{\perp} = k_{\perp}(\epsilon, k)$ . Here we used the notation

$$\begin{aligned} u_{1,2} &= D_p(\mp \sqrt{2}kl_B), \\ v_{1,2} &= \pm \frac{\sqrt{2}}{i|\epsilon|l_B} D_{p+1}(\mp \sqrt{2}kl_B), \\ w &= (k_{\perp} + ik)/|\epsilon|, \quad z = e^{2ik_{\perp}d}. \end{aligned} \quad (10)$$

Equation (9) must then be solved numerically, and leads to the energy bands  $\epsilon_n(k)$  shown in Fig. 2(a). For large  $|k|$ , the eigenvalues approach the well-known relativistic Landau levels at  $\epsilon l_B = \text{sgn}(n)\sqrt{2|n|}$  [2], including a zero-energy solution (not shown in Fig. 2).

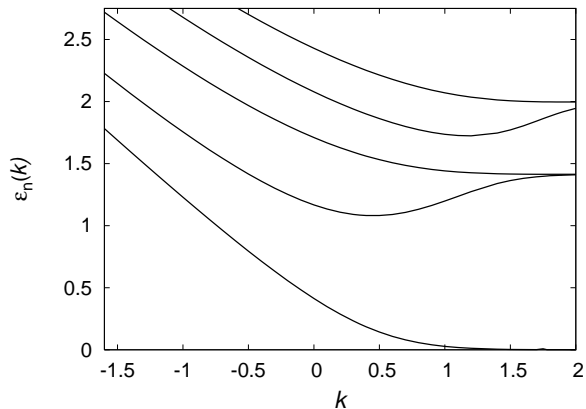


FIG. 3: Same as Fig. 2(a) but for  $\sigma = -1$ , cf. Fig. 1(b).

To illuminate the current-carrying states, we plot in Fig. 2(b) the transverse profile of the particle current,

$$j_{nk}(x) = v_F (\psi_{nk}^*(x))^T \sigma_2 \psi_{nk}(x), \quad (11)$$

where  $\psi_{nk}(x)$  is the transverse eigenspinor to energy  $\epsilon_n(k)$ . Generalizing the standard argument, see Appendix E in Ref. [17], to the case of Dirac-Weyl quasiparticles, one can show that

$$v_n(k) \equiv \int dx j_{nk}(x) = \partial_k \epsilon_n(k). \quad (12)$$

We stress that Eq. (12) is a nontrivial result for Dirac fermions. It holds for any magnetic field profile with  $B(x, y) = B(x)$ . This fact leads to the usual cancellation of carrier velocity  $v_n(k)$  and density of states  $(2\pi|\partial_k \epsilon_n(k)|)^{-1}$ , and thus the two-terminal conductance will be  $4e^2/h$  (assuming perfect contacts to reservoirs). However, as seen in Fig. 2(b), right- and left-moving states occupy the *same* spatial region and are therefore susceptible to backscattering perturbations, e.g. due to impurities, charge inhomogeneities, or fluctuations in the magnetic field. In practice, quantized conductance is thus not expected for a waveguide with  $B' = 0$ .

Next we consider the *asymmetric* case with  $\sigma = -1$  but still  $B' = 0$ , see Fig. 1(b). From the analogy to Schrödinger fermions, one expects to find special uni-directional *snake states* [15]. On a semi-classical level, the uni-directionality can be understood by noting that cyclotron orbits have a different winding sense for  $x < -d$  and  $x > d$ . The propagating snake state follows by combining half an orbit from each side and a linear trajectory in the central region. The energy quantization condition takes again the form (9) after replacing  $u_2 = D_{p+1}(-\sqrt{2}kl_B)$  and  $v_2 = \frac{\sqrt{2}}{i|\epsilon|l_B}(p+1)D_p(-\sqrt{2}kl_B)$  in Eq. (10). Numerical solution yields the spectrum depicted in Fig. 3. First, we notice a strong asymmetry in the energy bands  $\epsilon_n(k)$ , just as in the Schrödinger case [15]. For  $k < 0$  a linear dispersion relation is observed, corresponding to snake states propagating with

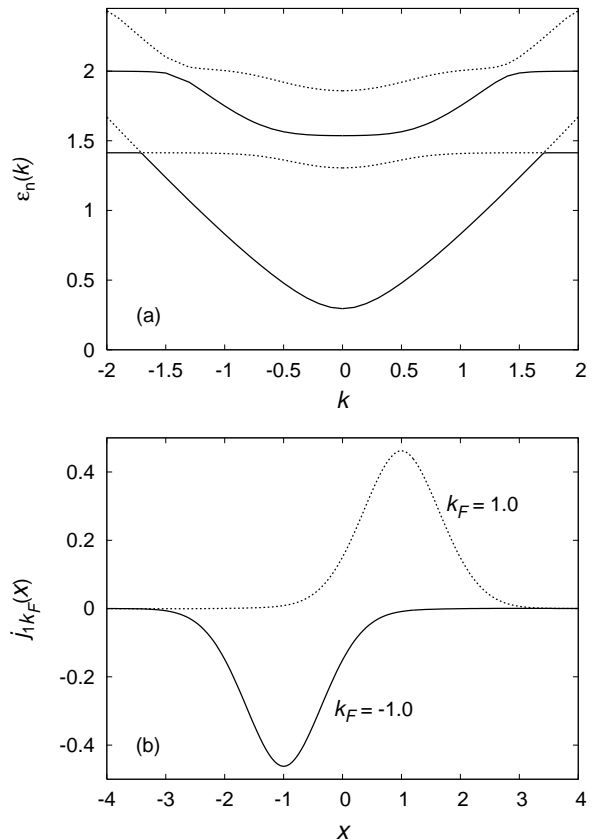


FIG. 4: (a) Same as Fig. 2(a) but for  $B' = -B$ , cf. Fig. 1(a). The lower pair of  $\epsilon_n(k)$  curves has an avoided level crossing (not visible on this scale). The current profile (b) at  $\epsilon l_B = 0.83$  (corresponding to  $k_F l_B \simeq \pm 1$ ) shows that the two counter-propagating snake states are spatially separated already for  $d = l_B$ .

$n$ -independent velocity  $|v_n| = v_F$  at sufficiently negative  $k$ , see Eq. (12). The equality of snake velocity and Fermi velocity for  $|kd| \gg 1$  also follows from a simple semiclassical estimate. Second, the levels merge pairwise at large positive  $k$  to form the relativistic Landau levels, except for the lowest band in Fig. 3 which merges with the highest negative- $\epsilon$  band (not shown) to approach the zero-energy Landau level. This is a new feature encountered only for Dirac fermions and makes this state easily identifiable for weakly doped graphene. However, it is important to stress that for any finite  $k$ , there can be *no* true zero-energy state for magnetic field configurations with  $\sigma = -1$ . This can be proven on general grounds as a consequence of the Aharonov-Casher theorem, which in turn follows as a special limit of the celebrated index theorem [18].

Interestingly, there is another peculiar subtlety for this magnetic field profile. This is seen by computing the equilibrium average of the current using Eqs. (11) and (12), which predicts a nonzero result. In fact, the equilibrium current formally diverges and is only limited by the bandwidth of the model. To interpret this non-sensical

result we note that in the absence of boundaries, the snake state propagates in just one direction and thus produces an *unbalanced current flow*. The conundrum is resolved when including boundary contributions to the current, which are inevitably present in any real sample. In fact, the dispersion relation in Fig. 3 ultimately bends upwards for  $k \rightarrow \infty$  in the presence of a boundary located at  $x_b \gg d$ . The counter-propagating edge state at this boundary will then balance the total current [15]. We have explicitly checked that this scenario holds true for the case of a zig-zag edge, where a simple boundary condition on the spinor at  $x = x_b$  can be used [3]. In analogy to quantum Hall edge states [8], however, it should be possible to experimentally probe the *locally* unbalanced current carried by the snake state using time-resolved transport measurements [19] or scanning tunneling spectroscopy.

We now go back to the *symmetric* setup  $\sigma = +1$  but take  $B' < 0$ . Such a field configuration can be generated by depositing two ferromagnetic layers on top of a graphene sheet covered by a thin insulating layer [10, 12]. In that case one finds two counter-propagating snake states, and no boundary contributions are required to get zero total current in equilibrium. While for  $B' = 0$ , no snake states exist, they do appear once  $B' < 0$ . By generalizing Eq. (9), numerical solution of the corresponding energy quantization condition leads to the results in Fig. 4(a). Qualitatively, the spectrum consists of snake states (with approximately linear dispersion) and Landau level states (dispersionless), with avoided level crossings between successive eigenenergies  $\epsilon_n(k)$ . If the Fermi level

intersects only the lowest band shown in Fig. 4(a), the quantized conductance  $4e^2/h$  follows directly from the Kubo formula. The current-carrying states at  $\pm k_F$  are counter-propagating snake states which are spatially separated and centered near  $x = \pm d$ , see Fig. 4(b). Due to this spatial separation, weak disorder effects or irregularities in the magnetic field will not be able to induce backscattering processes between these states as long as  $d \gtrsim l_B$ . In particular, snake states behave identically for both  $K$  valleys, and thus even inter-valley scattering processes are not expected to mix counter-propagating states. The conductance quantization in such a setup should therefore be observable and very precise.

To conclude, we have analyzed the properties of electron waveguides in graphene, produced by suitable inhomogeneous magnetic field profiles. Under the setup in Fig. 1(a) with  $B' < 0$ , we predict robust and highly accurate conductance quantization in units of  $4e^2/h$ . This system is clearly of interest in the context of interacting 1D quantum wire physics, as the electron-electron interaction can lead to qualitatively new features. We hope that our work motivates experimental and further theoretical studies.

We thank A. Altland, L. Erdős, T. Heinzl and J. Smet for discussions. T. K. G. is supported by the A. v. Humboldt foundation. R. E. is supported by the DFG (SFB Transregio 12), and by the ESF network INSTANS.

*Note added:* During the preparation of this manuscript, a preprint appeared [20] where some of our results for  $\sigma = -1$  were also reported.

- 
- [1] K.S. Novoselov *et al.*, Science **306**, 666 (2004); Nature **438**, 197 (2005); Y. Zhang, Y.W. Tan, H. Stormer, and P. Kim, Nature **438**, 201 (2005); C. Berger *et al.*, Science **312**, 1191 (2006).
- [2] For a recent review, see A.K. Geim and K.S. Novoselov, Nature Materials **6**, 183 (2007).
- [3] K. Nakada, M. Fujita, G. Dresselhaus, and M.S. Dresselhaus, Phys. Rev. B **54**, 17954 (1996); E. McCann and V.I. Fal'ko, J. Phys.: Cond. Matt. **16**, 2371 (2004); N.M.R. Peres, F. Guinea, and A.H. Castro Neto, Phys. Rev. B **73**, 125411 (2006); *ibid.* **73**, 241403(R) (2006); L. Brey and H.A. Fertig, Phys. Rev. B **73**, 235411 (2006); D.A. Abanin, P.A. Lee, and L.S. Levitov, Phys. Rev. Lett. **96**, 176803 (2006).
- [4] J.C. Meyer, A.K. Geim, M.I. Katsnelson, K.S. Novoselov, T.J. Booth, and S. Roth, Nature **446**, 60 (2007).
- [5] J.M. Pereira, V. Mlinar, F.M. Peeters, and P. Vasilopoulos, Phys. Rev. B **74**, 045424 (2006).
- [6] N.M.R. Peres, A.H. Castro Neto, and F. Guinea, Phys. Rev. B **73**, 195411 (2006); M.I. Katsnelson, Eur. Phys. J. B **57**, 225 (2007).
- [7] M.Y. Han, B. Özyilmaz, Y. Zhang, and P. Kim, Phys. Rev. Lett. **98**, 206805 (2007).
- [8] A.M. Chang, Rev. Mod. Phys. **75**, 1449 (2003).
- [9] P.D. Ye *et al.*, Phys. Rev. Lett. **74**, 3013 (1995).
- [10] For recent work, see M. Cerchez, S. Hugger, T. Heinzl, and N. Schulz, Phys. Rev. B **75**, 035341 (2007), and references therein.
- [11] For a review, see S.J. Lee, S. Souma, G. Ihm, and K.J. Chang, Phys. Rep. **394**, 1 (2004).
- [12] J. Smet, private communication.
- [13] D. Lawton, A. Nogaret, M.V. Makarenko, O.V. Kibis, S.J. Bending, and M. Henini, Physica E **13**, 699 (2002); M. Hara, A. Endo, S. Katsumoto, and Y. Iye, Phys. Rev. B **69**, 153304 (2004).
- [14] F.M. Peeters and A. Matulis, Phys. Rev. B **48**, 15166 (1993).
- [15] J.E. Müller, Phys. Rev. Lett. **68**, 385 (1992); S.M. Badalyan and F.M. Peeters, Phys. Rev. B **64**, 155303 (2001); N. Malkova, I. Gómez, and F. Domínguez-Adame, Phys. Rev. B **63**, 035317 (2001); J. Reijnders, A. Matulis, K. Chang, F.M. Peeters, and P. Vasilopoulos, Europhys. Lett. **59**, 749 (2002); H.-W. Lee and D.S. Novikov, Phys. Rev. B **68**, 155402 (2003).
- [16] A. De Martino, L. Dell'Anna, and R. Egger, Phys. Rev. Lett. **98**, 066802 (2007).
- [17] N.W. Ashcroft and N.D. Mermin, *Solid State Physics* (Saunders Coll., Philadelphia, 1976).
- [18] Y. Aharonov and A. Casher, Phys. Rev. A **19**, 2461 (1979); L. Erdős and V. Vougalter, Comm. Math. Phys. **225**, 299 (2002).

- [19] N.B. Zhitenev, R.J. Haug, K. v. Klitzing, and K. Eberl, Phys. Rev. Lett. **71**, 2292 (1993); G. Ernst, N.B. Zhitenev, R.J. Haug, and K. v. Klitzing, Phys. Rev. Lett. **79**, 3748 (1997).
- [20] P. Rakyta, L. Oroszlany, A. Kormanyos, C.J. Lambert, and J. Cserti, preprint cond-mat/0707.3974.